INFLUENCE OF EXTERNAL DISTURBANCES AND COMPRESSIBILITY ON FREE TURBULENT MIXING

By Youn H. Oh* and Dennis M. Bushnell
NASA Langley Research Center

SUMMARY

It has been shown that disturbances in external flow can significantly affect, by as much as an order of magnitude, the turbulent mixing rate in free shear layers. A particularly important finding is the fact that the length scale of the external flow disturbances is as important as the amplitude. Also a single parameter correlates the change in entrainment rate remarkably well. The difference between the effect of wide-band and narrow-band disturbances is stressed. The inclusion of the model for pressure fluctuation term in the kinetic energy equation in a two-equation model predicts the reduced spreading rate in high Mach number, high Reynolds number, adiabatic, free turbulent shear layers.

INTRODUCTION

The free turbulent shear layer is a relatively simple flow which is useful for verification of turbulence modeling and has many practical applications such as design of jet engine combustors, slot injection, and gas-dynamic lasers. The requirements of these devices generally vary. The combustor and gas laser require fast mixing and slot flows need slow mixing to be effective as thermal shields or to provide drag reduction.

Of importance in engineering design of such devices is the determination of the relative importance of various parameters upon mixing rate, and whether one can "control" the entrainment. The rate of free turbulent mixing primarily depends on the level and scale of turbulence in the shear layer. There are many things that can affect the structure of free turbulence; for example, large rates of strain and impinging shocks, etc. The purpose of the present investigation is to determine the effect of free-stream disturbances when both free-stream turbulence intensity and scale are varied, and also to determine the influence of Mach number on the entrainment rate of free shear layers. The influence of free-stream disturbances may be particularly important in ground simulation of combustor flows, especially scramjets, where the free-stream flow is heated

*NASA-ODU Research Associate.

by a variety of devices such as arc or vitiated burners which probably produce fairly large disturbance levels and scales. (See fig. 1.)

Experimentalists often fail to measure the intensity of such free-stream disturbances and very rarely measure the dominant or characteristic scale. High Mach number is also found to be a very important factor that affects turbulent free mixing structure. The 1972 Langley Conference on Free Turbulent Shear Flows (ref. 1) indicated that the data on spreading rate for turbulent free shear layers contain disagreement between data and "theory" of up to a factor of 3 or more for supersonic Mach numbers, the larger disagreement occurring at the higher Mach numbers ($M \approx 3$ to 5).

External or free-stream disturbances can be roughly divided into two important classes. The first class is generally referred to as acoustic disturbances. These are isentropic pressure waves having the following characteristics: The magnitudes of pressure, density, and velocity fluctuations are related to each other isentropically (up to moderate amplitude). These disturbances are highly directional, propagate with the speed of sound, and can be transmitted and reflected by the shear layer. This type of disturbance is known to affect laminar shear layer and combustion stability.

Extensive reviews of existing literature on acoustic disturbances can be found in Rockwell (ref. 2) and Borisov and Rozenfel'd (ref. 3). Important experimental data (ref. 4) showing the effect of narrow-band acoustic mode disturbances on fully turbulent shear layers are shown in figure 2 and are discussed in detail in the main body of the paper, particularly in reference to turbulence control.

The second important class of external disturbances is usually referred to as free-stream vorticity or "turbulence." Both of these classes of disturbances can be either wide band or narrow band. Wide-band disturbances generally have typical turbulence spectra. Vinogradov et al. (ref. 5) found the core length of two-dimensional coflowing jets to be strongly affected (factor of 4 difference in spreading rate) by the type of screen applied upstream of the external flow. Rodi (ref. 6) also reports similar findings (Vagt (1970) and Patel (1970)). The present paper describes a study of the effect of wide-band disturbances, employing an equation for the scale of turbulence since disturbances in the "free-stream" (on either or both sides of the mixing layer) would generally have distinct scales which are not related to the local scale of the shear layer. A parametric study of the effect of scale and intensity of free-stream disturbances is presented so that, for example, one can assess the influence of tunnel disturbances on free-flight simulation of scramjet engines. (See fig. 1.)

The present numerical solution of the free turbulent shear layer employs a "two-equation" turbulence model, a turbulent kinetic energy equation for the intensity, and a dissipation equation for the length scale of turbulence. A model for the pressure-velocity correlation term, representing a "compressibility" effect, which was developed by Oh

(ref. 7), based on an eddy-shock-wave concept is included in the turbulent kinetic energy model equation for predictions of the influence of high Mach number upon entrainment in free shear layers.

SYMBOLS

a	mass fraction of species
c_p	specific heat
e	turbulent kinetic energy, $\frac{1}{2}(u''^2 + v''^2 + w''^2)$
f	frequency
H	total enthalpy, $\sum_{i=1}^{n} c_{p,i} a_i T + \frac{1}{2} u^2$
L	reference length
l	length scale
l_{in}	integral length scale
M	Mach number; also grid size
n	total number of species; also exponent of isotropic turbulence energy initial decay law
$N_{Pr,e}$	ratio of turbulent diffusivity in turbulent kinematic energy equation to that of mean momentum
$N_{Pr,t}$	turbulent Prandtl number
$N_{Pr,\epsilon}$	ratio of turbulent diffusivity in dissipation equation to that of mean momentum
p	static pressure
R	gas constant; also Reynolds number

$N_{Sc,t}$ turbulent Schmidt number

T static temperature

u velocity component in x-direction

u_s local sonic speed

v velocity component in y-direction

w velocity component normal to u and v

X_o virtual origin of velocity similarity profiles

x coordinate parallel to outside flows (fig. 1)

x_c core length of jet

x_o initial x where initial conditions are specified

y coordinate normal to x (fig. 3)

$y_{.5}$ y where $(\tilde{u} - \tilde{u}_2)/(\tilde{u}_1 - \tilde{u}_2) = 0.5$

β $= \left(\overline{M}^2 - 1\right)^{1/2} \Big/ \overline{M}$

γ ratio of specific heat

δ shear layer width parameter, $\left|y_{\tilde{u}=0.1} - y_{\tilde{u}=0.9}\right| \Big/ L$

δ_o $= \delta$ at $x = x_o$

ϵ dissipation rate of turbulent kinetic energy

Λ computed shear layer width referred to that implied by linear spreading law with computed σ and X_o, $\left|y_{\tilde{u}=\sqrt{0.1}} - y_{\tilde{u}=\sqrt{0.9}}\right| \Big/ \left[1.32(x - X_o)/\sigma\right]$

λ $\equiv 0.875\delta_o$

μ_e eddy viscosity

ρ density

σ similarity parameter used as a measure of spreading rate

σ_0 σ for low-speed constant-density flows

σ_* $\equiv \lim_{\sqrt{\tilde{e}_\infty} l_\infty \to 0} \sigma$

ϕ $\equiv \frac{\tilde{u}_1 + \tilde{u}_2}{\tilde{u}_1 - \tilde{u}_2}\left[\frac{\sqrt{e_\infty}}{\tilde{u}_1 - \tilde{u}_2}\right]_{x=0}\left[\frac{l_\infty}{\lambda}\right]_{x=0}$

Subscripts and superscripts:

1 conditions on high-velocity side external flow

2 conditions on low-velocity side external flow

i species i

i,j tensor indices

max maximum value

∞ conditions outside of shear layer

$(\bar{\ })$ conventional temporal mean

$(\ )'$ (instantaneous) - $(\bar{\ })$

$(\tilde{\ })$ mass-averaged temporal mean

$(\ )''$ (instantaneous) - $(\tilde{\ })$

GOVERNING EQUATIONS AND ASSUMPTIONS

The physical problem is depicted schematically in figure 3. The shear layer is formed between two parallel uniform flows of different velocities. The higher velocity is called $\tilde{u}_1$ and the slower stream velocity is denoted by $\tilde{u}_2$. The X-axis is alined with the external uniform flows and the Y-axis is the direction normal to the uniform flow. (The flow properties vary most rapidly in the y-direction.) In the subsequent analysis, mass-averaged dependent variables, proposed by Favre (ref. 8), are used for most flow properties. Mass-averaged values are represented by a superscript tilde (~). The following relationships hold:

$$\tilde{u} = \bar{u} + \frac{\overline{\rho' u'}}{\bar{\rho}}$$

$$u'' = u' - \frac{\overline{\rho' u'}}{\bar{\rho}}$$

so that $\overline{\rho u} = \overline{\rho}\tilde{u}$. Both independent and dependent variables are used in their primitive form. The governing equations employed cover both multispecies and high-speed mixing.

Simplifying Assumptions

The following assumptions are made:

(1) The flow is steady on the average

(2) The Reynolds number is sufficiently high so that the mixing layer is fully turbulent and molecular diffusion can be neglected compared with turbulent diffusion

(3) The axial pressure gradient is zero

(4) No chemical reactions occur

Basic Equations

The typical free shear layer with no extraneous strain has an order of magnitude difference in the derivatives of the flow properties in the x- and y-direction and allows the usual boundary-layer-type (quasi-parallel) approximations. The conservation equations describing the problem for the mean flow quantities may be written in the following form (ref. 8):

Continuity:

$$\frac{\partial(\overline{\rho}\tilde{u})}{\partial x} + y^{-J}\frac{\partial\left(y^{J}\overline{\rho}\tilde{v}\right)}{\partial y} = 0 \qquad (1)$$

"x" mean momentum:

$$\bar{\rho}\tilde{u}\frac{\partial\tilde{u}}{\partial x} + \bar{\rho}\tilde{v}\frac{\partial\tilde{u}}{\partial y} + y^{-J}\frac{\partial\left(y^{J}\overline{\rho u''v''}\right)}{\partial y} = 0 \tag{2}$$

"y" mean momentum:

$$\frac{\partial\bar{p}}{\partial y} + \frac{\partial\left(\overline{\rho v''^{2}}\right)}{\partial y} = 0 \tag{3}$$

Mean energy:

$$\bar{\rho}\tilde{u}\frac{\partial\tilde{H}}{\partial x} + \bar{\rho}\tilde{v}\frac{\partial\tilde{H}}{\partial y} - y^{-J}\frac{\partial\left(y^{J}\overline{\rho H''v''}\right)}{\partial y} = 0 \tag{4}$$

Species:

$$\bar{\rho}\tilde{u}\frac{\partial\tilde{a}_i}{\partial x} + \bar{\rho}\tilde{v}\frac{\partial\tilde{a}_i}{\partial y} + y^{-J}\frac{\partial\left(y^{J}\overline{\rho a_i''v''}\right)}{\partial y} = 0 \qquad (i = 1, 2, \ldots, n) \tag{5}$$

Equation of state:

$$\bar{\rho} = \frac{\gamma_1\bar{p}}{(\gamma_1 - 1)\tilde{T}\left(\sum_{i=1}^{n} R_i\tilde{a}_i\right)} \tag{6}$$

In these equations all the variables are rendered dimensionless by referring all lengths to L, velocities to $\tilde{u}_1$, pressure to $\bar{\rho}_1\tilde{u}_1^2$, density to $\bar{\rho}_1$, temperature to $\tilde{u}_1^2/c_{p,1}$, total enthalpy to $\tilde{u}_1^2$, specific heat to $c_{p,1}$ $\left(c_{p,i} = \sum_{i=1}^{n} c_{p,1,i}a_{1,i}\right)$, and gas constant to R_1 $\left(R_1 = \sum_{i=1}^{n} R_{1,i}a_{1,i}\right)$. The exponent $J = 0$ for two-dimensional and $J = 1$ for axisymmetric shear layers.

Closure Assumptions

The preceding set of equations are not closed because the turbulent correlations are unknown. Boussinesq's eddy viscosity model is assumed to describe the turbulent shear stress; that is, $\overline{\rho u''v''} = -\mu_e\partial\tilde{u}/\partial y$ along with Prandtl's energy model for the eddy viscosity, $\mu_e = C_\mu l\bar{\rho}\tilde{e}$, where C_μ is a modeling constant and $\tilde{e}$ is the turbulence kinetic energy $\tilde{e} = \overline{\rho(u''^2 + v''^2 + w''^2)}/\bar{\rho}$. Also $\overline{\rho H''v''}/(\partial\tilde{H}/\partial y)$ and $\overline{\rho a_i''v''}/(\partial\tilde{a}_i/\partial y)$ are assumed to be proportional to the eddy viscosity (by constant factors); that is,

$\overline{\rho a'' v''} = \frac{\mu_e}{N_{Sc,t}} \frac{\partial \tilde{a}}{\partial y}$ and $\overline{\rho H'' v''} = \frac{\mu_e}{N_{Pr,t}} c_p \frac{\partial \tilde{T}}{\partial y} + \frac{\mu_e}{N_{Sc,t}} \tilde{T} \left(\sum_{i=1}^{n} c_{p,i} \frac{\partial \tilde{a}_i}{\partial y} \right) + \overline{\rho u} \mu_e \frac{\partial \tilde{u}}{\partial y}$ where

$N_{Sc,t}$ and $N_{Pr,t}$ are the turbulent Schmidt and Prandtl number, respectively.

Turbulence Model

Prandtl's energy model for the eddy viscosity requires the turbulence kinetic energy and length scale. Often the length scale is algebraically related to the width of shear layer itself and yields a reasonable result for the free shear layer. But, in order to study the effect of external disturbances which have their own scale (which is not related to the shear layer), use of an equation governing evolution of the scale of turbulence is essential. Thus a "two-equation" model approach is the minimum necessary to describe the turbulence field in the present problem. The equation for the turbulence dissipation rate is used to compute the turbulence scale. There are other equations which would serve the same purpose, such as a vorticity equation (ref. 9) or an equation for the quantity, energy-times-length scale (ref. 10). Actually, these equations are all very similar (ref. 11).

Equations derived from the Navier-Stokes equations to describe turbulence energy and dissipation include a number of unknown correlations. Modeling of these unknowns requires a delicate balance between mathematical rigor and physical intuition since elaborate mathematical manipulation can be meaningless if not supported by experimental measurement. In general, the higher order correlations in the turbulent kinetic equation are better known than those in the equations for the length scale (ref. 12). Most notoriously difficult to measure, and hence least known of the turbulent fluctuating properties, are the pressure fluctuation terms. A model for the pressure-velocity correlation hypothesized by Oh (ref. 7) is included in the kinetic energy equation. No attempt was made to model pressure fluctuation terms in the dissipation equation. The model used by Spalding's group with their constants (ref. 1) was used herein for the dissipation equation. The final model equations are as follows:

Turbulent kinetic energy:

$$\overline{\rho u} \frac{\partial \tilde{e}}{\partial x} + \overline{\rho v} \frac{\partial \tilde{e}}{\partial y} - y^{-J} \frac{\partial}{\partial y} \left(y^J \frac{\mu_e}{N_{Pr,e}} \frac{\partial \tilde{e}}{\partial y} \right) - \mu_e \left(\frac{\partial \tilde{u}}{\partial y} \right)^2 + C_{e,1} \overline{\rho} D\tilde{e} + \overline{\rho} \epsilon$$

$$- C_{e,2} H(\overline{M} - 1) \beta \tilde{e} \left[\overline{\rho} D + \operatorname{sign}\left(\frac{\partial \overline{M}}{\partial y} \right) u_s \beta \frac{\partial \overline{\rho}}{\partial y} - \beta u_s^{-1} \frac{\partial \overline{\rho}}{\partial y} \right] = 0 \qquad (7)$$

Turbulent dissipation equation:

$$\overline{\rho u} \frac{\partial \epsilon}{\partial x} + \overline{\rho v} \frac{\partial \epsilon}{\partial y} - y^{-J} \frac{\partial}{\partial y} \left(y^J \frac{\mu_e}{N_{Pr,\epsilon}} \frac{\partial \epsilon}{\partial y} \right) - C_{\epsilon,1} \frac{\epsilon}{\tilde{e}} \mu_e \left(\frac{\partial u}{\partial y} \right)^2 + \frac{C_{\epsilon,2} \overline{\rho} \epsilon^2}{\tilde{e}} = 0 \qquad (8)$$

where $J = 0$ for two-dimensional and $J = 1$ for axisymmetric shear layers, H is the Heaviside unit function $H(\zeta) = 0$ when $\zeta < 0$ and $H(\zeta) = 1$ when $\zeta \geq 0$. Also, the following definitions are used: $D \equiv \partial\tilde{u}/\partial x + \partial\tilde{v}/\partial y$; u_s = Local sonic speed; $\beta \equiv \left(\overline{M}^2 - 1\right)^{1/2}/\overline{M}$; $\epsilon \equiv \tilde{e}^{3/2}/l$ so that $\mu_e = C_\mu \overline{\rho}\tilde{e}^2/\epsilon$. The constants used are $C_\mu = 0.09$, $N_{Sc,t} = 0.7$, $N_{Pr,t} = 0.9$, $N_{Pr,e} = 1.0$, $N_{Pr,\epsilon} = 1.3$, $C_{e,1} = 0$, $C_{e,2} = 0.14$, $C_{\epsilon,1} = 1.43$, and $C_{\epsilon,2} = 1.92$.

Initial and Boundary Conditions

Initial conditions.- Initial profiles of all dependable variables are required to start the solution procedure. All the results reported in this paper are computed with a set of initial profiles which were "guessed at" based upon the physics of the flow. The scarcity of experimental data, especially measured profiles for the turbulence energy and length scale, is the reason for using "arbitrary" (but physically reasonable) initial profiles. The quasi-similarity (all the computed results show linear shear layer growth, see fig. 5) of the results is a posteriori justification, that is, the calculations proceeded far enough downstream for the influence of the starting profiles to be "washed out." The initial profiles are generated as follows: First axial velocity $\tilde{u}$ profiles are generated for a given width parameter $\delta_o = \dfrac{\left|y_{\tilde{u}=0.1} - y_{\tilde{u}=0.9}\right|_{x=0}}{L}$

$$\tilde{u}(0,y) = \frac{1}{2}\left[(\tilde{u}_1 + \tilde{u}_2) + (\tilde{u}_1 - \tilde{u}_2)\mathrm{erf}(\zeta)\right] \tag{9}$$

where $\zeta = 2 \times 0.90621514 y/\delta_o$. Then

$$\tilde{e}(0,y) = \underbrace{\frac{1}{2}\left[(\tilde{e}_1 + \tilde{e}_2) + \left|\tilde{e}_1 - \tilde{e}_2\right|\mathrm{erf}(\zeta)\right]}_{\tilde{e}_{fr}} + \underbrace{\frac{1}{2}\left\{\left[\tilde{e}_{max,sh} - \frac{1}{2}(\tilde{e}_1 + \tilde{e}_2)\right]\exp\left(-2\zeta^2\right)\right\}}_{\tilde{e}_{sh}} \tag{10}$$

where the first term $\tilde{e}_{fr}$ is the contribution of free-stream disturbances and the second term $\tilde{e}_{sh}$ is chosen as the contribution of mean shear $\left(\text{from the assumed relation } \tilde{e} \propto \left(\frac{d\tilde{u}}{dy}\right)^2 \text{ when } \tilde{e}_1 = \tilde{e}_2 = 0\right)$. The term $\tilde{e}_{max,sh}$ is another input which is chosen as 0.12 for most incompressible cases and as 0.08 for supersonic cases. The term $\tilde{e}_{sh}$ was neglected when $\tilde{e}_1 + \tilde{e}_2 > 2\tilde{e}_{max,sh}$. Note that these equations are in nondimensional form. In order to estimate dissipation, the distribution of length scale is computed as

$$l(0,y) = \underbrace{\frac{\frac{1}{2}\left[(l_1 + l_2) + |l_1 - l_2|\,\mathrm{erf}(\zeta)\right]\tilde{e}_{fr}}{\tilde{e}}}_{l_{fr}} + \underbrace{\frac{\lambda\tilde{e}_{max,sh} - \frac{1}{4}(l_1 + l_2)(\tilde{e}_1 + \tilde{e}_2)}{\tilde{e}_{max,sh} - \frac{1}{2}(\tilde{e}_1 + \tilde{e}_2)}\,\frac{\tilde{e}_{sh}}{\tilde{e}}}_{l_{sh}} \tag{11}$$

where $\lambda \equiv 0.875\delta_o$ and $l_{sh} = 0$ when $\tilde{e}_{max,sh} < \frac{1}{2}(\tilde{e}_1 + \tilde{e}_2)$. Then ϵ is computed as $\epsilon = \tilde{e}^{3/2}/l$. Total enthalpy is assumed to be initially uniform

$$\tilde{H}(0,y) = 1$$

The static temperature is obtained from the expression

$$\tilde{T}(0,y) = \left[\left(1 + \frac{\gamma - 1}{2}\overline{M}_1^2\right)\tilde{H} - \frac{\gamma - 1}{2}\overline{M}_1^2\tilde{u}^2\right]\frac{\gamma}{c_p(\gamma - 1)R} \tag{12}$$

For static pressure, normal velocity and density, the initial assumptions include:

$$\left.\begin{aligned} \overline{p}(0,y) &= p_\infty \\ \tilde{v}(0,y) &= 0 \\ \overline{\rho}(0,y) &= \overline{M}_1^2\,\frac{p}{\tilde{T}R} \end{aligned}\right\} \tag{13}$$

Boundary conditions.- The external free stream usually contains some type of disturbance. The major disturbances can be divided into two broad groups, acoustic and vortical. The effect of narrow-band acoustic disturbances is fundamentally different than that of free-stream vorticity (turbulence). The present research effort is concerned with the effect of wide-band-type free-stream turbulence only.

The free-stream turbulence could be the result of upstream agitation, diffusion from an adjoining shear layer (wall boundary layer in enclosed flow or free shear layer in case of coaxial jet, etc.), or distributed sources such as chemical reaction or distributed fine obstacles, etc. (that is, dust flows). The most well documented data are for decaying isotropic turbulence. (A good example is grid-generated turbulence.) Therefore, the boundary conditions for the kinetic energy and dissipation equation are limited to isotropic decaying turbulence in the present study.

Batchelor and Townsend (ref. 13) found grid-generated isotropic turbulence decays in the early stage as

$$\frac{\tilde{e}}{u_\infty^2} = B\left(\frac{x}{M} - \frac{x_g}{M}\right)^{-1}$$

$$\frac{l_{in}}{M} = C\left(\frac{x}{M} - \frac{x_g}{M}\right)^{1/2}$$

where A, B, and C are constants, and l_{in}, x_g, and M are the integral length scale, grid location, and grid size, respectively.

In order to study the variation of boundary conditions for the turbulence model equations with x, the turbulence energy is assumed to vary as

$$\tilde{e}_\infty = \tilde{u}_\infty{}^2 A\left(\frac{x}{M} - \frac{x_g}{M}\right)^n$$

In the absence of mean shear, the model equation for the turbulent kinetic energy equation becomes

$$\tilde{u}_\infty \frac{d\tilde{e}_\infty}{dx} = -\epsilon \tag{14}$$

Substituting the expression for $\tilde{e}_\infty$ results in

$$\epsilon = -\tilde{u}_\infty{}^3 \frac{n}{M} A\left(\frac{x}{M} - \frac{x_g}{M}\right)^{n-1} \tag{15}$$

From the relation $l = \frac{\tilde{e}^{3/2}}{\epsilon}$

$$l = -\frac{MA^{1/2}}{n}\left(\frac{x}{M} - \frac{x_g}{M}\right)^{\frac{n}{2}+1} \tag{16}$$

Initial boundary conditions are therefore

$$(\tilde{e}_\infty)_{x=0} = \tilde{u}_\infty{}^2 A\left(\frac{x_0}{M} - \frac{x_g}{M}\right)^n \tag{17}$$

$$(l_\infty)_{x=0} = -\frac{MA^{1/2}}{n}\left(\frac{x_0}{M} - \frac{x_g}{M}\right)^{\frac{n}{2}+1} \tag{18}$$

From equations (14), (15), (17), and (18),

$$\tilde{e}_\infty = (\tilde{e}_\infty)_{x=0}\left\{1 - \left[\frac{x - x_0}{(l_\infty)_{x=0}{}^n}\right]^n \left[\frac{(\tilde{e}_\infty)_{x=0}}{\tilde{u}_\infty{}^2}\right]^{n/2}\right\} \tag{19}$$

$$\epsilon_\infty = \frac{\left(\tilde{e}_\infty^{3/2}\right)_{x=0}}{(l_\infty)_{x=0}} \left\{ 1 - \left[\frac{x - x_o}{(l_\infty)_{x=0}^{n}} \right]^{n-1} \left[\frac{(\tilde{e}_\infty)_{x=0}}{\tilde{u}_\infty^{2}} \right]^{n-\frac{1}{2}} \right\} \tag{20}$$

The recent measurements made by Comte-Bellot and Corrisin (ref. 14) show that $n \approx -1.25$.

Symmetric boundary conditions are imposed on the X-axis in the axisymmetric and two-dimensional jet cases. (Center velocity is allowed to decrease.)

Numerical solution procedure.- The numerical method used to solve the governing equation is the implicit finite-difference method of Crank-Nicholson with the dependent variables in conservation form. Linearization is accomplished by initially lagging the nonlinear coefficient a step and then integrating until convergence.

Variable grid spacing is used in the y-direction. The spacing was increased by a geometrical progression on each side of the shear layer center line. In order to prevent the shear region from outgrowing the computing net, the computing net was continuously expanded in the y-direction by doubling the grid spacing whenever the converged solution for $\tilde{u}$ changes by a predetermined margin at both edges for the pure shear layer case and at the outer edge for the jet case. A typical run, 250 cross-node points and 170 marching steps in x ($\approx$100 times the initial thickness δ_o distance), for the incompressible binary mixing case takes approximately 200 seconds of CPU time on the CDC 6600 computer system. Sixty percent of this time is actually spent in solving the finite-difference equations and the rest of the machine time is spent in data management and plotting routines. A solution for the supersonic shear layer takes approximately three times longer than for an incompressible case. Convergence was tested on $\tilde{u}$, $\tilde{v}$, and $\tilde{e}$ with a convergence criterion 0.1 percent relative (or combined with an equivalent absolute criterion for $\tilde{v}$).

RESULTS AND DISCUSSION

Comparison With Data

Experimental data which can be used to check the validity of the present prediction are extremely scarce. Most often, data are incomplete, that is, the intensity of free-stream disturbances is measured but not the characteristic scale. Also, the core length of the jet may be measured but not the initial boundary-layer thickness (ref. 5), etc.

Thus the comparison with incomplete data becomes no more than finding the missing data which would yield agreement in the results. Nevertheless Rodi (ref. 6) demonstrated, by using a prediction method similar to the present one, that the measured effect of free-stream disturbances (Patel (1970) and Vagt (1970)) on free turbulent mixing could be qual-

itatively simulated. In this vein, a comparison will be made with the Vinogradov et al. (ref. 5) experiment. The experimental setup (see fig. 4) consisted of an enclosed two-dimensional channel with two separating plates which initially divided the channel into three equal size ducts. The ratio of center duct velocity to the velocity of two outer ducts was varied along with the "agitating grids" in the outlet sections of the ducts. The experiment determined the variation of core length of the center jet with velocity ratio and initial intensity of turbulence for incompressible isothermal flow. From the present authors' viewpoint, the data have the following defects: (1) The wall shear layers on either side of the splitter plate were not measured. (The core length depends not only on the spreading rate but also on the virtual origin, that is, initial shear layer thickness.) (2) The core length was measured from schlieren photographs, with smoke in the center jet. However, the end of the core was not defined clearly, that is, whether the concentration was $a_1 = 0.99$ or 0.9, etc. The analytical determination of x_c depends greatly on such a criterion. (3) The location where the grids are placed is not certain. If the grids were placed at the exit of the jet as the article (ref. 5) implies, then the results would have been considerably affected by the immediate wake of the grid. (4) The outer uniform flow carries not only decaying grid-generated turbulence but also turbulence diffused from the outer wall boundary layer. (The nature of such turbulence is much less well known than grid turbulence.) (5) The initial free-stream turbulence energy was measured but the scales were not. However, because of the lack of more complete data, comparisons will be shown for this case by using plausible assumptions.

A number of predictions were made with arbitrary but reasonable initial shear layer widths for the no grid case. (See circle symbol in fig. 4.) The prediction and experimental data are compared in figure 4. The flow quantities assumed in predictions of all cases are $\tilde{u}_1 = 30$ m/sec, $\delta_0 = 0.5875 \times 2$ cm, definition for the core length $\tilde{a}_1 = 0.98$, length scale for the no grid case $l_\infty/\lambda = 1.0$, and Δl_∞ is assumed to be proportional to the grid spacing (or rod diameter). The implication of this comparison is the slope of the no grid case data with velocity ratio is used to define the end of core as $\tilde{a}_1 = 0.98$, the x_c at $\tilde{u}_2/\tilde{u}_1 = 0.3$ for the no grid case is used to calibrate the initial shear layer width $\delta_0 = 0.5875 \times 2$, and the grids with 2-mm rod and 4-mm rod are used to fix $\Delta(l_\infty/\lambda)/(2\text{-mm rod diam}) = 0.15$. Therefore, the results for the 8-mm grid can be looked upon as the real comparison, which is certainly very reasonable and tends to vindicate the present approach.

Parametric Study of Effect of Free-Stream Disturbances

Because of the lack of complete data, the comparison of the present results with experiment is quantitatively inconclusive (but qualitatively satisfactory) as the attempt in the previous section demonstrates.

In this section a parametric study is made of the effect of the intensity and length scale of wide-band-type free-stream disturbances on 2-D incompressible, free, turbulent air-air mixing. A number of computer runs were made with identical flow conditions except for variations in velocity ratio $\tilde{u}_2/\tilde{u}_1$, turbulent intensity $\sqrt{\tilde{e}_\infty}/\tilde{u}_\infty$, and length scale l_∞/λ. All computed cases are summarized in table I with the results σ and X_0.

To show the effects of $\tilde{e}_\infty$ and l_∞ on profiles of shear layer properties, samples of the similarity profiles $\tilde{u}$, $\tilde{e}$, and l/λ as functions of $\sigma y/(x - X_0)$ and $\tilde{u}_{max}$, $\tilde{e}_{max}$, and $\overline{uv}_{max}$, and Λ as a function of x (which represent large disturbances, very small disturbances, and effects of disturbance on both sides of the shear layer and on just one side alone) are shown in figure 5. The spreading parameter σ which is used as the measure for the spreading (see fig. 3) is defined herein by the relation (ref. 15) $\sigma = 1.32/\Delta\eta$ where $\Delta\eta$ is the angular distance between two rays when $(\tilde{u} - \tilde{u}_2)/(\tilde{u}_1 - \tilde{u}_2) = (0.1)^{1/2}$ and $(\tilde{u} - \tilde{u}_2)/(\tilde{u}_1 - \tilde{u}_2) = (0.9)^{1/2}$. The accompanying virtual origin is X_0. The quantities σ and X_0 are evaluated from the last $\tilde{u}$ profile computed and a profile at about $x = 0.8$ of the total distance computed. A single parameter which can be used to compare the rate of spreading of all properties in all flow conditions is not yet known. The parameter σ and other parameters (ref. 16) have their limitations. The quantity σ can be used to compare the growth rate of velocity width (also momentum thickness and entrainment rate for constant-density shear layers) only when the velocity profiles are similar. But the presence of a high level of turbulence in the external flow distorts the profiles; however, they are "self-similar." The self-similar velocity profile for the quiet boundary condition case (fig. 5(a)) is similar to that of Liepmann and Laufer (ref. 17). (A comparison can be found in ref. 7.) The presence of high $\tilde{e}_1$ makes the self-similar velocity profile smoother near the high-velocity side because of the increased shear stress. (See fig. 5(e).) The presence of high free-stream disturbances on both sides stretches the profile at both ends so that the self-similar profile becomes nearly similar again. (Compare figs. 5(a) and 5(i).) The σ values used in table I, figure 6, and figure 7 can be regarded as comparing approximately 80 percent of the momentum thickness because of the way it is defined.

In the course of this study, the following qualitative observations were made: (1) The effects on turbulence intensity is approximately proportional to $\sqrt{\tilde{e}_\infty}/(\tilde{u}_1 - \tilde{u}_2)$; that is, for a given $\sqrt{\tilde{e}_\infty}/\tilde{u}_\infty$, the effects of disturbances in the high-velocity side became more prominent and the effects of external turbulence on the low-velocity side diminishes as $\tilde{u}_2/\tilde{u}_1$ decreases. The higher $\tilde{u}_2/\tilde{u}_1$, the more sensitive the flow is to external disturbances. (2) As $l_\infty \to 0$ and $\sqrt{\tilde{e}_\infty} \to 0$, σ and X_0 approach an asymptotic value. (3) The overall profiles are quasi-similar (i.e., though turbulence properties are still changing the mean velocity profiles are similar) in most of the cases computed even though the boundary conditions imposed are strongly nonsimilar. Note the constancy of $\Lambda = \left|y_{\tilde{u}=\sqrt{0.1}} - y_{\tilde{u}=\sqrt{0.9}}\right| \Big/ \left[1.32(x - X_0)/\sigma\right]$ as a function of X (linear spreading) in fig-

ures 5(d), 5(h), 5(l), and 5(p). (4) Very small $\sqrt{\tilde{e}_\infty}$ causes numerical instability near the edge due to the definition $l = \frac{\tilde{e}^{3/2}}{\epsilon}$. (5) The ratios of diffusivities in $\tilde{e}$ and $\tilde{\epsilon}$ equations have to have a certain value, that is, 1.3 (as Spalding's group used). Otherwise the length scale profile would exhibit an anomalous dip or peak near the edge of the shear layer. (6) Disturbances on the low-velocity side of the external flow can further increase mixing rate up to 10 percent over the correlated results shown in figure 6.

Surprisingly, a single parameter

$$\phi = \frac{\tilde{u}_1 + \tilde{u}_2}{\tilde{u}_1 - \tilde{u}_2}\left(\frac{\sqrt{\tilde{e}_{\infty,1}}}{\tilde{u}_1 - \tilde{u}_2}\right)_{x=0}\left(\frac{l_\infty}{\lambda}\right)_{x=0}$$

correlates the variation of σ/σ_* with "one side" external disturbances as shown in figure 6.

Here σ_* is the limiting value of σ for small ϕ. (Actual σ_* values used are marked in the table.) It should be noted that the present calculations, as correlated in figure 6, indicate potentially large effects of free-stream disturbance on spreading rate for simple shear layers (factor of up to 10 change in spreading rate possible).

In figure 7, predictions made with $\left(\frac{\sqrt{\tilde{e}_1}}{\tilde{u}_1 - \tilde{u}_2}\frac{l_1}{\lambda}\right)_{x=0} = 1.7$ and 0 are plotted with experimental data collected by Birch and Eggers (ref. 1) in the format suggested by Kline for σ as a function of $\tilde{u}_2/\tilde{u}_1$. This comparison suggests that the disturbances in the facility free stream were responsible for at least some of the data scatter which is more than 100 percent at the high velocity ratios $\left(\tilde{u}_2/\tilde{u}_1 \to 1\right)$.[1]

The effect of narrow-band acoustic disturbances could be markedly different from the effects of the wide-band vorticity type so far considered. The difference is very well demonstrated in the experiment conducted by Vlasov and Ginevsky (ref. 4). The experimental setup and the results were shown in figure 2. Narrow-band acoustic disturbances generated by a loud speaker were injected into a fully turbulent free subsonic jet. The center-line velocity decay with x is plotted for the no-sound case and two different disturbance frequencies. The data show that the external disturbances not only accelerate mixing (low-frequency disturbance), but could also attenuate mixing (high-frequency input). This is a very significant result and indicates that the mixing rate can be controlled by artificially inputting narrow-band disturbances. It is currently planned to study this phenomenon with a spectral plane analysis.

---

[1]Note that the slow rate of development to a "pure shear layer" is also conjectured (ref. 16) for the large scatter of data as $\tilde{u}_2/\tilde{u}_1 \to 1$.

Influence of Mach Number

Oh (ref. 7) modeled the pressure-velocity correlation term $\overline{p' \frac{\partial u^j}{\partial x^j}}$ in the kinetic energy equation based on an eddy shock-wave concept. The prediction (ref. 7) made by a one-equation model was reasonably good. The same cases were computed again with the dissipation equation included. (Note that the p' terms are not yet included in the dissipation equation.)

A prediction with $C_{e,2} = 0.14$ (equivalent to $C_5C_6 = 0.07$ of ref. 7) are shown in figure 8. The plots of σ against $\overline{M}_1$ are qualitatively similar to the results of the one-equation method (ref. 7). Detailed profile comparisons indicate the need for slightly higher diffusivity in the dissipation equation which is a possible indication of the need for a model of the p' term in that equation.

To be noted is that all the data shown in figure 9 are from relatively "clean" configurations. The data that have some sort of wall proximity, which may allow reflection of large noise levels back into the shear layer or allow self generation of low-frequency narrow-band noise such as cavity flows, are excluded. These "noisy flows" generally spread faster. (See fig. 9.)

CONCLUDING REMARKS

It has been shown that disturbances in external flow can significantly affect, by as much as an order of magnitude, the free turbulent mixing rate in shear layers. A particularly important finding is the fact that the length scale of the external flow disturbances is as important as the amplitude.

Also, a single parameter correlates the change in entrainment rate remarkably well. The difference between the effect of wide-band and narrow-band disturbances is stressed. The inclusion of the model for the velocity-pressure correlation term in the kinetic energy equation in a two-equation model predicts the reduced spreading rate in high Mach number, high Reynolds number, adiabatic, free turbulent shear layers.

REFERENCES

1. Anon.: Free Turbulent Shear Flows. Vol. I – Conference Proceedings. NASA SP-321, 1973.

2. Rockwell, Donald O.: The Macroscopic Nature of Jet Flows Subjected to Small Amplitude Periodic Disturbances. Sonochem. Eng., vol. 67, no. 109, 1971, pp. 99-107.

3. Borisov, Yu. Ya.; and Rozenfel'd, É. I.: Action of Acoustic Oscillations on Flow Stability and Structure. Soviet-Phys.-Acoustics, vol. 17, no. 2, Oct.-Dec. 1971, pp. 154-168.

4. Vlasov, Ye. V.; and Ginevskiy, A. S.: Generation and Suppression of Turbulence in an Axisymmetric Turbulent Jet in the Presence of an Acoustic Influence. NASA TT F-15,721, 1974.

5. Vinogradov, Yu. V.; Gruzdev, V. N.; and Talanlov, A. V.: Effect of the Intensity of Turbulence Upon the Process of Mixing Slipstreams at a Different Ratio of Velocities. FTD-HT-23-866-74, U.S. Air Force, Apr. 15, 1974. (Available from DDC as AD 778 798.)

6. Rodi, Wolfgang: The Prediction of Free Turbulent Boundary Layers by Use of a Two-Equation Model of Turbulence. Ph. D. Thesis, Imperial College (London), Dec. 1972.

7. Oh, Y. H.: Analysis of Two-Dimensional Free Turbulent Mixing. AIAA Paper No. 74-594, June 1974.

8. Favre, A.: Statistical Equations of Turbulent Gases. Problems of Hydrodynamics and Continuum Mechanics. Soc. Indust. & Appl. Math., 1969, pp. 231-266.

9. Saffman, P. G.: A Model for Inhomogeneous Turbulent Flow. Proc. Roy. Soc. (London), ser. A, vol. 317, no. 1530, June 1970, pp. 417-433.

10. Rotta, J. C.: Recent Attempts To Develop a Generally Applicable Calculation Method for Turbulent Shear Flow Layers. Turbulent Shear Flows, AGARD-CP-93, Jan. 1972, pp. A-1 – A-11.

11. Wolfshtein, M.; Naot, D.; and Lin, A.: Models of Turbulence. Rep. ME-746(N), Ben-Gurion Univ. Negev (Israel), June 1974.

12. Bradshaw, P. (appendix by V. C. Patel): The Strategy of Calculation Methods for Complex Turbulent Flows. I. C. Aero Rep. 73-05, Aeronaut. Dep., Imp. Coll. Sci. & Technol., Aug. 1973.

13. Batchelor, G. K.; and Townsend, A. A.: Decay of Isotropic Turbulence in the Initial Period. Proc. Roy. Soc., ser. A, vol. 193, no. 1032, Apr. 22, 1948, pp. 539-558.

14. Comte-Bellot, Geneviève; and Corrsin, Stanley: The Use of a Contraction To Improve the Isotropy of Grid-Generated Turbulence. J. Fluid Mech., vol. 25, pt. 4, Aug. 1966, pp. 657-682.

15. Brown, Garry; and Roshko, Anatol: The Effect of Density Difference on the Turbulent Mixing Layer. Turbulent Shear Flows, AGARD-CP-93, Jan. 1972, pp. 23-1 – 23-12.

16. Brown, Garry L.; and Roshko, Anatol: On Density Effects and Large Structure in Turbulent Mixing Layers. J. Fluid Mech., vol. 64, pt. 4, July 1974, pp. 775-816.

17. Liepmann, Hans Wolfgang; and Laufer, John: Investigations of Free Turbulent Mixing. NACA TN 1257, 1947.

18. Maydew, R. C.; and Reed, J. F.: Turbulent Mixing of Axisymmetric Compressible Jets (in the Half-Jet Region) With Quiescent Air. SC-4764(RR), Sandia Corp. (Albuquerque, N. Mex.), Mar. 1963.

19. Sirieix, M.; and Solignac, J. L.: Contribution à l'Etude Expérimentale de la Couche de Mélange Turbulent Isobare d'un Ecoulement Supersonique. Separated Flows, pt. I, AGARD CP No. 4, May 1966, pp. 241-270.

20. Ikawa, Hideo: Turbulent Mixing Layer Experiment in Supersonic Flow. Ph. D. Thesis, California Inst. Technol., 1973.

21. Morrisette, E. Leon; and Birch, Stanley F.: Mean Flow and Turbulent Measurements in a Mach 5 Shear Layer. Pt. I – The Development and Spreading of the Mean Flow. Fluid Mechanics of Mixing, Earl M. Uram and Victor W. Goldschmidt, eds., Amer. Soc. Mech. Eng., c.1973, pp. 79-86.

22. Hill, W. G., Jr.; and Page, R. H.: Initial Development of Turbulent, Compressible, Free Shear Layers. Trans. ASME, Ser. D: J. Basic Eng., vol. 91, no. 1, Mar. 1969, pp. 67-73.

23. Rhudy, J. P.; and Magnan, J. D., Jr.: Turbulent Cavity Flow Investigation at Mach Numbers 4 and 8. AEDC-TR-66-73, U.S. Air Force, June 1966. (Available from DDC as AD 483 748.)

24. Fernandez, F. L.; and Zukoski, E. E.: Experiments in Supersonic Turbulent Flow With Large Distributed Surface Injection. AIAA J., vol. 7, no. 9, Sept. 1969, pp. 1759-1767.

25. Rudy, David H.; and Birch, Stanley F.: Mean Flow Development and Surface Heating for an Attaching Compressible Free Shear Layer. J. Spacecraft & Rockets, vol. 11, no. 5, May 1974, pp. 348-351.

26. Cary, Aubrey M., Jr.; and Hefner, Jerry N.: Film-Cooling Effectiveness and Skin Friction in Hypersonic Turbulent Flow. AIAA J., vol. 10, no. 9, Sept. 1972, pp. 1188-1193.

27. Kenworthy, Michael; and Schetz, Joseph A.: An Experimental Study of Slot Injection Into a Supersonic Stream. NASA CR-2128, 1973.

28. Drewry, J. E.; Neer, M. E.; and Scaggs, N. E.: Supersonic Mixing and Combustion Studies of Ducted Hydrogen-Air Flows at an Inlet Air Mach Number of 2.6. AIAA Paper No. 73-1320, Nov. 1973.

TABLE I.- COMPUTED RESULTS OF SPREADING RATE AS A FUNCTION OF FREE-STREAM DISTURBANCES

Flow conditions for data given in table.

$\tilde{u}_1 = 30$ cm/sec

$T_{total} = 318$ K

$p_{total} = 1$ atm

$M_1 = 0.084$

R/cm = 17296.5802

$\delta_o = 0.3$ cm $\equiv \left| y_{\tilde{u}=1} - y_{\tilde{u}=0.9} \right|_{x=0}$

All cases computed from $x_o = 0$ to $x = 30$ cm $(100\delta_o)$

Varied conditions, at $x = x_o$

$\frac{\tilde{u}_2}{\tilde{u}_1} = 0.5, 0.3, 0.6, 0.9$

$\frac{\sqrt{\tilde{e}_\infty}}{u_\infty} = 0.005$ to $\sqrt{0.03}$

$\frac{l_\infty}{\lambda} = 0.1$ to 10 $\quad (\lambda = 0.875\delta_o)$

(a) $\frac{\tilde{u}_2}{\tilde{u}_1} = 0.05$; $\frac{\sqrt{\tilde{e}_{\infty,2}}}{\tilde{u}_2} = 0.02$; $\frac{l_{\infty,2}}{\lambda} = 0.1$

$\frac{l_{\infty,1}}{\lambda}$	Value of σ and $\frac{x_o}{\lambda}$ for $\frac{\sqrt{\tilde{e}_{\infty,1}}}{\tilde{u}_1}$ of –			
	0.06	0.086	0.1	$\sqrt{0.03}$
1		[a]14.14 -13.41		
4	13.83 -12.99		13.72 -15.01	12.83 -23.47
6	13.69 -12.84		13.10 -16.00	12.24 -24.23
10	13.54 -12.69		12.73 -15.73	

[a]Used as σ_* in figure 6.

TABLE I. - COMPUTED RESULTS OF SPREADING RATE AS A FUNCTION OF FREE-STREAM DISTURBANCES – Continued

(b) $\frac{\tilde{u}_2}{\tilde{u}_1} = 0.3$; $\frac{\sqrt{\tilde{e}_{\infty,2}}}{\tilde{u}_2} = 0.005$; $\frac{l_{\infty,2}}{\lambda} = 0.01$

$\frac{l_{\infty,1}}{\lambda}$	Value of σ and $\frac{X_0}{\lambda}$ for $\frac{\sqrt{\tilde{e}_{\infty,1}}}{\tilde{u}_1}$ of –			
	0.0377	0.06	0.1	$\sqrt{0.03}$
1	23.13 -20.76		23.26 -26.59	
4		21.92 -21.90	20.86 -27.50	19.39 -38.55
6		21.92 -21.37	20.05 -27.31	18.06 -39.73
10		21.07 -21.03	19.01 -26.10	16.26 -38.36

(c) $\frac{\tilde{u}_2}{\tilde{u}_1} = 0.3$; $\frac{\sqrt{\tilde{e}_{\infty,1}}}{\tilde{u}_1} = \frac{\sqrt{\tilde{e}_{\infty,2}}}{\tilde{u}_2}$; $\frac{l_{\infty,1}}{\lambda} = \frac{l_{\infty,2}}{\lambda}$

$\frac{l_{\infty,1}}{\lambda}$	Value of σ and $\frac{X_0}{\lambda}$ for $\frac{\sqrt{\tilde{e}_{\infty,1}}}{\tilde{u}_1}$ of –			
	0.06	0.1	$\sqrt{0.02}$	$\sqrt{0.03}$
0.1				[a]23.36 -9.79
1				22.22 -26.78
2		21.89 -26.10		21.05 -33.75
4	21.86 -21.98	20.74 -27.73	19.78 -34.40	19.21 -39.70
6	21.44 -21.52	19.92 -27.62		17.85 -41.03
10	21.01 -21.26	18.88 -26.63	17.10 -34.13	15.99 -39.62

[a]Used as σ_* in figure 6.

TABLE I.- COMPUTED RESULTS OF SPREADING RATE AS A FUNCTION OF FREE-STREAM DISTURBANCES – Continued

(d) $\frac{\tilde{u}_2}{\tilde{u}_1} = 0.6$; $\frac{\sqrt{\tilde{e}_{\infty,2}}}{\tilde{u}_2} = 0.005$; $\frac{l_{\infty,2}}{\lambda} = 0.1$

$\frac{l_{\infty,1}}{\lambda}$	Value of σ and $\frac{X_0}{\lambda}$ for $\frac{\sqrt{\tilde{e}_{\infty,1}}}{\tilde{u}_1}$ of –			
	0.05	0.06	0.1	$\sqrt{0.03}$
0.1			[a]49.58 -25.83	
1	46.88 -46.06		46.05 -53.56	
4		40.57 -46.48	36.05 -55.85	30.86 -77.98
6		38.73 -45.33	32.90 -53.56	26.58 -79.12
10				[b]21.36 -95.12

[a]Used as σ_* in figure 6.

[b]Similarity profiles are included in figure 5.

(e) $\frac{\tilde{u}_2}{\tilde{u}_1} = 0.6$; $\frac{\sqrt{\tilde{e}_{\infty,1}}}{\tilde{u}_1} = \frac{\sqrt{\tilde{e}_{\infty,2}}}{\tilde{u}_2}$; $\frac{l_{\infty,1}}{\lambda} = \frac{l_{\infty,2}}{\lambda}$

$\frac{l_{\infty,1}}{\lambda}$	Value of σ and $\frac{X_0}{\lambda}$ for $\frac{\sqrt{\tilde{e}_{\infty,1}}}{\tilde{u}_1}$ of –					
	0.005	0.6	0.1	$\sqrt{0.015}$	$\sqrt{0.02}$	$\sqrt{0.03}$
0.1	[a]49.35 -43.81					
1				43.86 -54.36		
4		39.44 -45.60	34.00 -54.59			28.52 -87.43
10	42.20 -43.92				[a]22.79 -63.58	[a]19.71 -98.48

[a]Similarity profiles are included in figure 5.

TABLE I.- COMPUTED RESULTS OF SPREADING RATE AS A FUNCTION OF FREE-STREAM DISTURBANCES – Continued

(f) $\frac{\tilde{u}_2}{\tilde{u}_1} = 0.6$; $\frac{2\sqrt{\tilde{e}_{\infty,2}}}{\tilde{u}_2} = \frac{\sqrt{\tilde{e}_{\infty,1}}}{\tilde{u}_1}$; $\frac{l_{\infty,2}}{\lambda} = \frac{l_{\infty,1}}{\lambda}$

$\frac{l_{\infty,1}}{\lambda}$	Value of σ and $\frac{X_o}{\lambda}$ for $\frac{\sqrt{\tilde{e}_{\infty,1}}}{\tilde{u}_1}$ of –		
	0.06	0.1	$\sqrt{0.03}$
4	40.27 -46.74	35.56 -55.96	29.99 -76.08
6	38.22 -45.03	32.22 -54.74	26.18 -75.24
10	36.03 -42.97	28.56 -50.59	20.42 -101.98

(g) $\frac{\tilde{u}_2}{\tilde{u}_1} = 0.9$; $\frac{\sqrt{\tilde{e}_{\infty,2}}}{\tilde{u}_2} = 0.005$; $\frac{l_{\infty,2}}{\lambda} = 0.1$

$\frac{l_{\infty,1}}{\lambda}$	Value of σ and $\frac{X_o}{\lambda}$ for $\frac{\sqrt{\tilde{e}_{\infty,1}}}{\tilde{u}_1}$ of –				
	0.00526	0.05	0.06	0.1	$\sqrt{0.03}$
0.1	[a]209.47 -179.09				
1		145.61 -153.14			
4			65.71 -122.25	50.31 -117.14	38.91 -116.34
6			53.07 -117.45	40.17 -112.38	31.17 -113.33
10			40.41 -111.35	30.55 -108.84	23.67 -110.55

[a]Used as σ_* in figure 6.

TABLE I.- COMPUTED RESULTS OF SPREADING RATE AS A FUNCTION OF FREE-STREAM DISTURBANCES – Concluded

(h) $\frac{\tilde{u}_2}{\tilde{u}_1} = 0.9$; $\frac{\sqrt{\tilde{e}_{\infty,1}}}{\tilde{u}_1} = \frac{\sqrt{\tilde{e}_{\infty,2}}}{\tilde{u}_2}$; $\frac{l_{\infty,1}}{\lambda} = \frac{l_{\infty,2}}{\lambda}$

$\frac{l_{\infty,1}}{\lambda}$	Value of σ and $\frac{X_0}{\lambda}$ for $\frac{\sqrt{\tilde{e}_{\infty,1}}}{\tilde{u}_1}$ of –	
	0.005	$\sqrt{0.03}$
0.1	209.37 -179.20	
1	199.09 -168.19	
10		23.87 -112.38

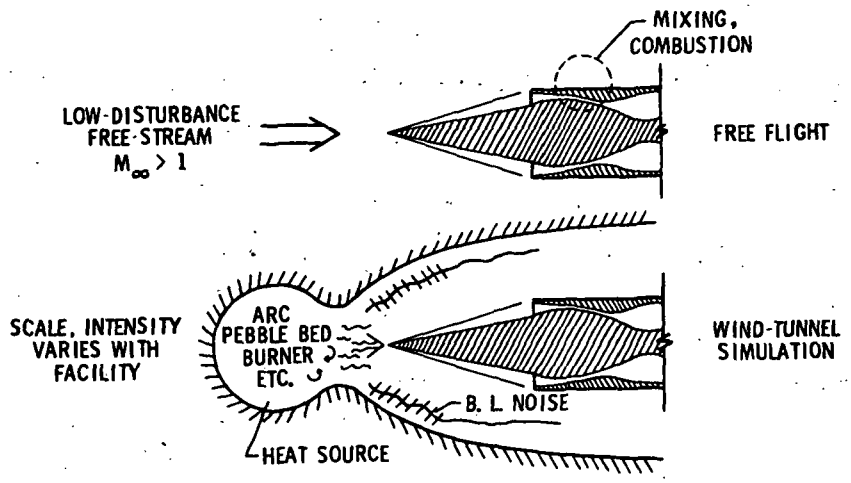

Figure 1.- Schematic of Ramjet/Scramjet engine ground simulation.

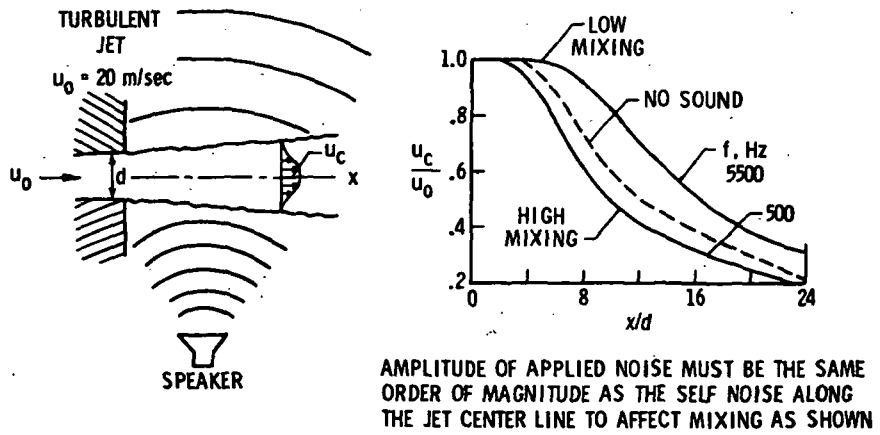

Figure 2.- Effect of narrow-band disturbances.

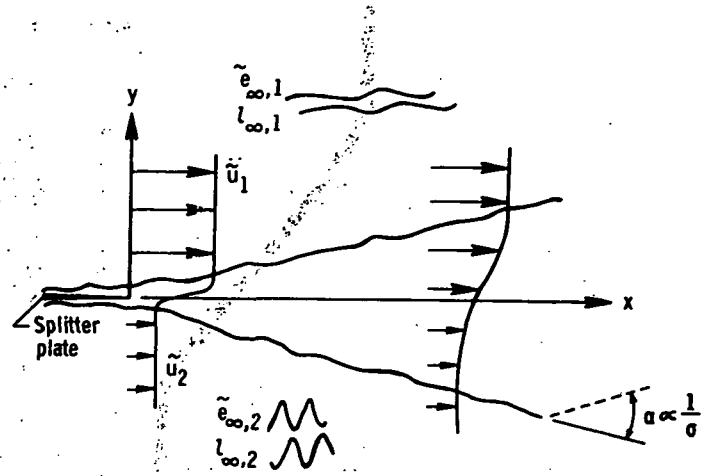

Figure 3.- Sketch of problem.

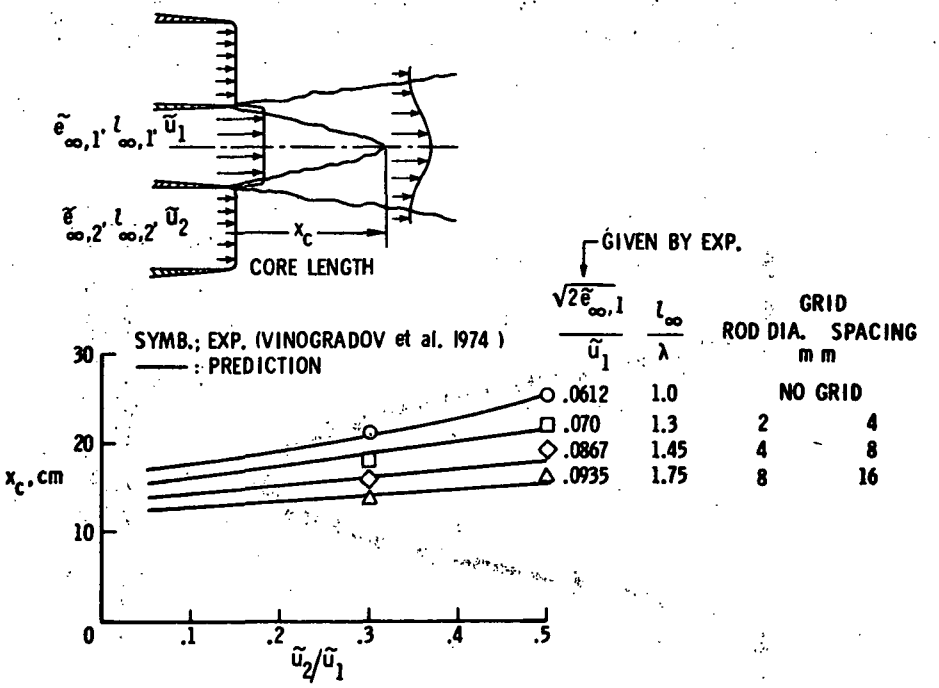

Figure 4.- Effect of wide-band free-stream disturbances on turbulent free mixing (low speed) comparison with data.

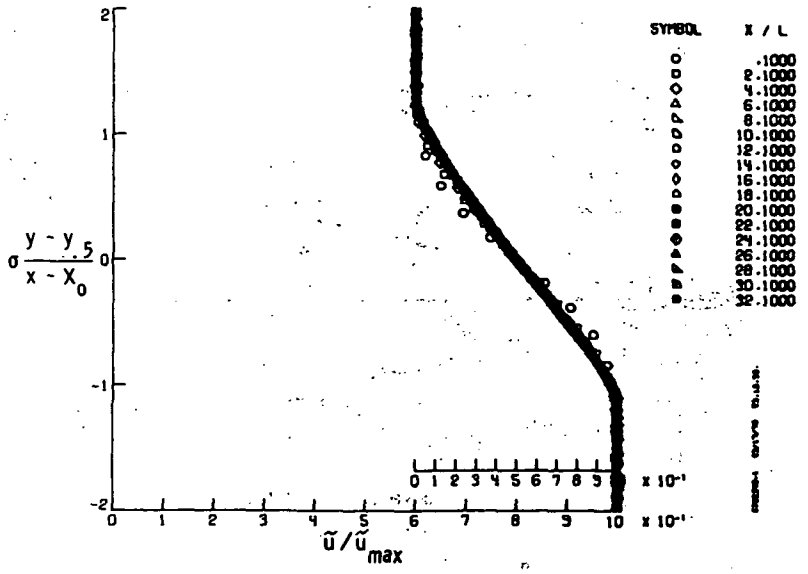

(a) Variation of $\tilde{u}/\tilde{u}_{max}$ with $\sigma(y - y_{.5})/(x - X_0)$ for $\tilde{u}_2/\tilde{u}_1 = 0.6$ with turbulence boundary conditions at $x = 0$; $\sqrt{\tilde{e}_\infty}/\tilde{u}_\infty = 0.005$; $l_\infty/\lambda = 0.1$; $L = \frac{10}{3}\delta_0$; $X_0/L = -11.5034$; $\sigma = 49.3547$.

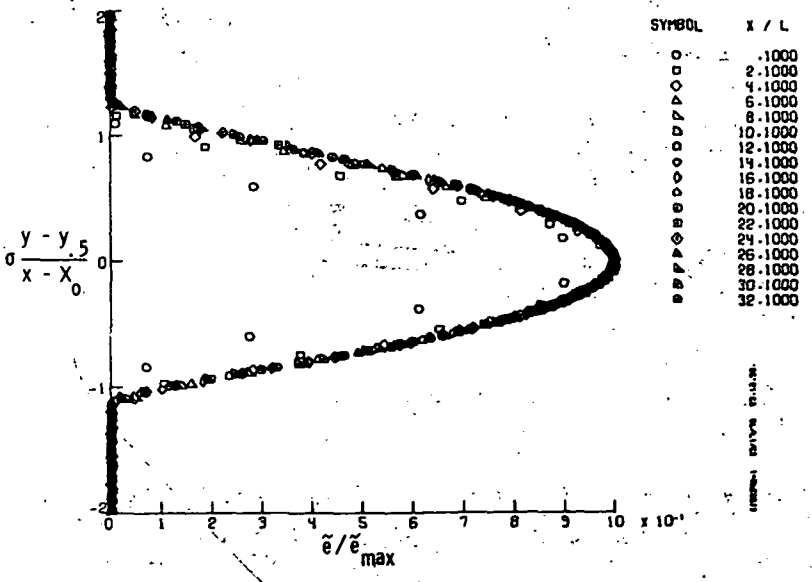

(b) Variation of $\tilde{e}/\tilde{e}_{max}$ with $\sigma(y - y_{.5})/(x - X_0)$. $X_0/L = 11.5034$; $\sigma = 49.3547$.

Figure 5.- Computed profiles.

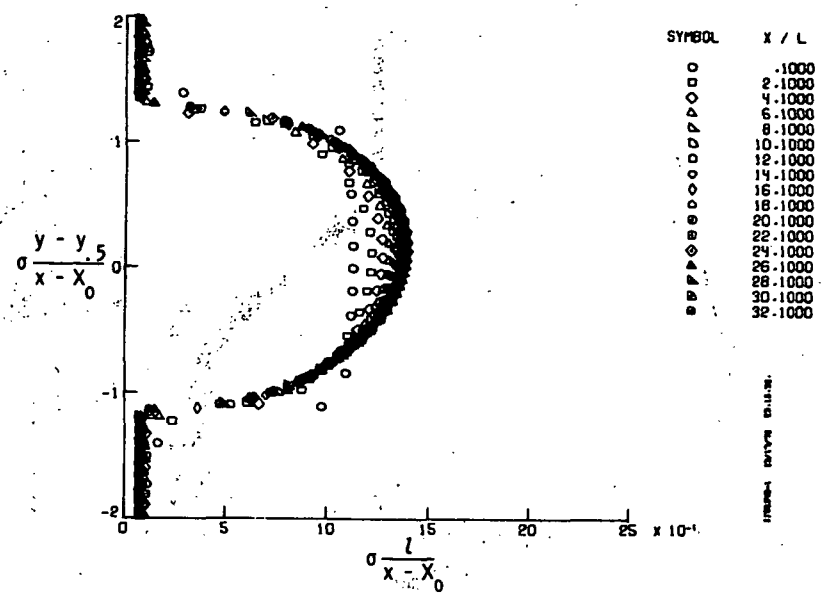

(c) Variation of $\sigma l/(x - X_0)$ with $\sigma(y - y_{.5})/(x - X_0)$. $X_0/L = -11.5034$; $\sigma = 49.3547$.

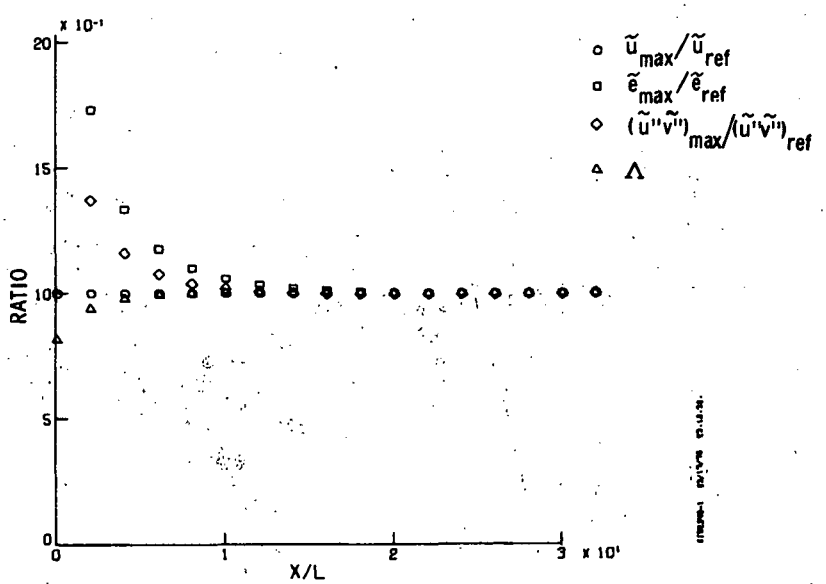

(d) Variation of $\tilde{u}_{max}/\tilde{u}_{ref}$, $\tilde{e}_{max}/\tilde{e}_{ref}$, $(\tilde{u}''\tilde{v}'')_{max}/(\tilde{u}''\tilde{v}'')_{ref}$, and Λ with x/L. $\sqrt{\tilde{e}_{ref}}/(\tilde{u}_1 - \tilde{u}_2) = \sqrt{0.0311}$; $(\tilde{u}''\tilde{v}'')_{ref}/(\tilde{u}_1 - \tilde{u}_2)^2 = 0.0108$; $L = \frac{10}{3}\delta_0$; $X_0/L = -11.5034$; $\sigma = 49.3547$.

Figure 5.- Continued.

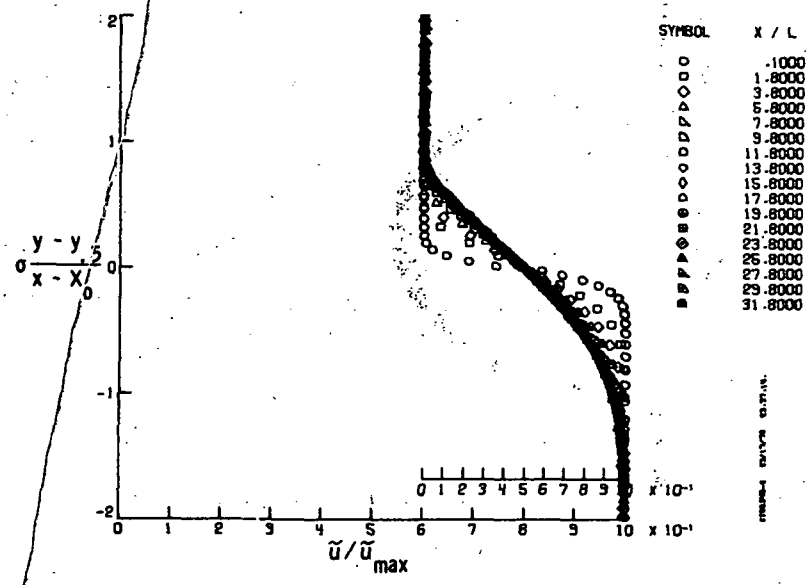

(e) Variation of $\tilde{u}/\tilde{u}_{max}$ with $\sigma(y - y_{.5})/(x - X_0)$ for $\tilde{u}_2/\tilde{u}_1 = 0.6$ with turbulence boundary conditions at $x = 0$; $\sqrt{\tilde{e}_{\infty,1}}/\tilde{u}_1 = \sqrt{0.03}$; $l_{\infty,1}/\lambda = 10$; $\sqrt{\tilde{e}_{\infty,2}}/\tilde{u}_2 = 0.005$; $l_{\infty,2}/\lambda = 0.1$; $L = \frac{10}{3}\delta_0$; $X_0/L = -24.9709$; $\sigma = 21.3565$.

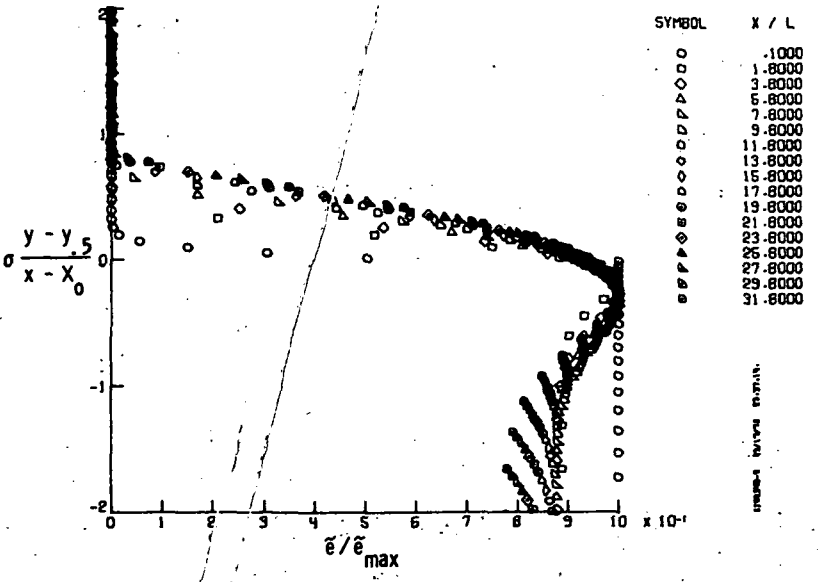

(f) Variation of $\tilde{e}/\tilde{e}_{max}$ with $\sigma(y - y_{.5})/(x - X_0)$. $X_0/L = -24.9707$; $\sigma = 21.3565$.

Figure 5.- Continued.

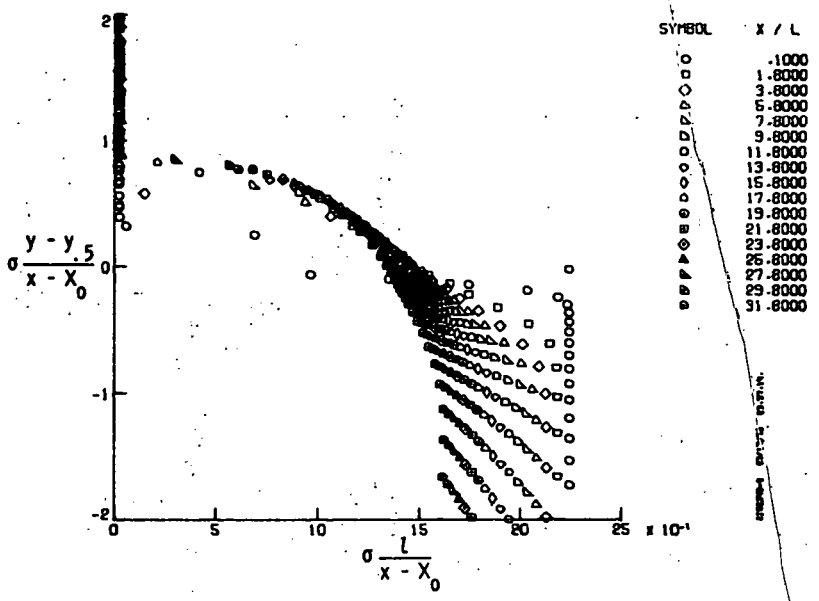

(g) Variation of $\sigma l/(x - X_0)$ with $\sigma(y - y_{.5})/(x - X_0)$. $X_0/L = -24.9707$; $\sigma = 21.3565$.

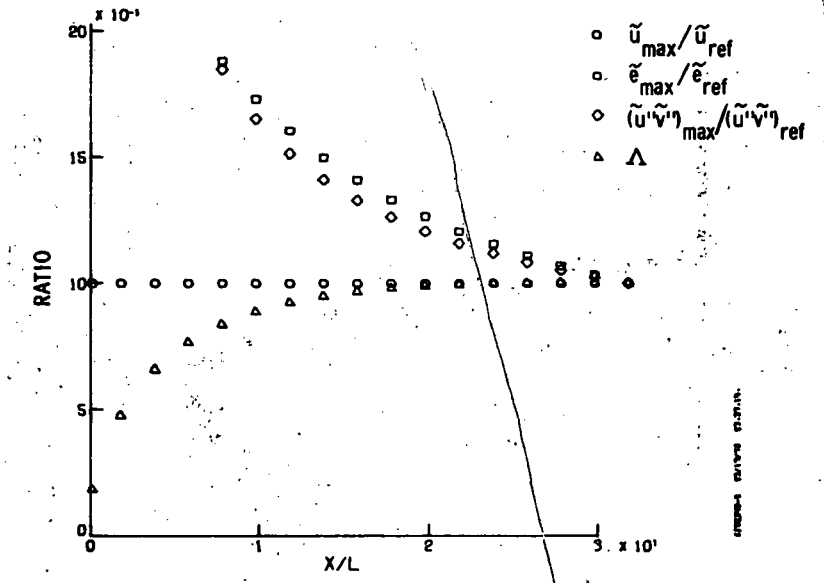

(h) Variation of $\tilde{u}_{max}/\tilde{u}_{ref}$, $\tilde{e}_{max}/\tilde{e}_{ref}$, $(\tilde{u}''\tilde{v}'')_{max}/(\tilde{u}''\tilde{v}'')_{ref}$, and Λ with x/L. $\sqrt{\tilde{e}_{ref}}/(u_1 - u_2) = \sqrt{0.0754}$; $(\tilde{u}''\tilde{v}'')_{ref}/(u_1 - u_2)^2 = 0.0212$; $L = \frac{10}{3}\delta_0$; $X_0/L = -24.9707$; $\sigma = 21.3565$.

Figure 5.- Continued.

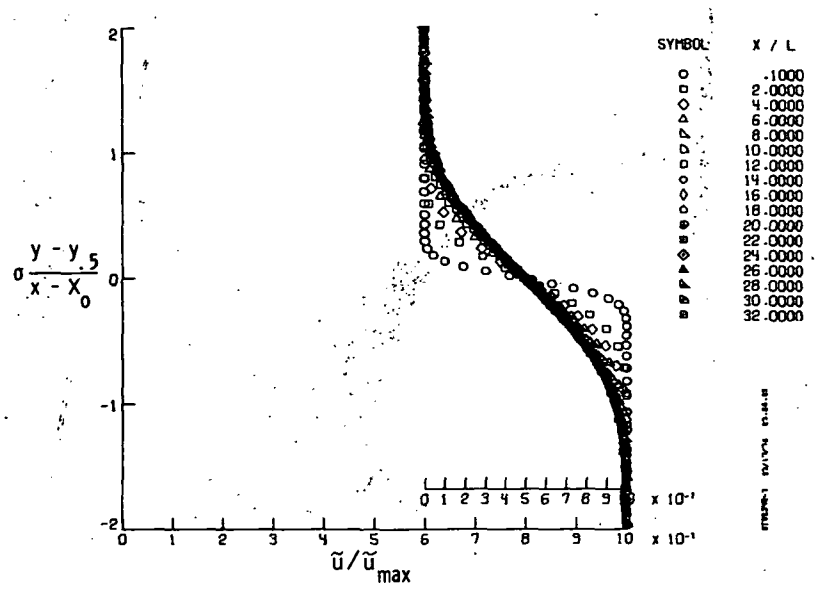

(i) Variation of $\tilde{u}/\tilde{u}_{max}$ with $\sigma(y - y_{.5})/(x - X_0)$ for $\tilde{u}_2/\tilde{u}_1 = 0.6$ with turbulence boundary conditions at $x = 0$; $\sqrt{\tilde{e}_\infty}/u_\infty = \sqrt{0.03}$; $\ell_\infty/\lambda = 10$; uniform initial length scale profile; $X_0/L = -25.8005$; $\sigma = 19.7200$.

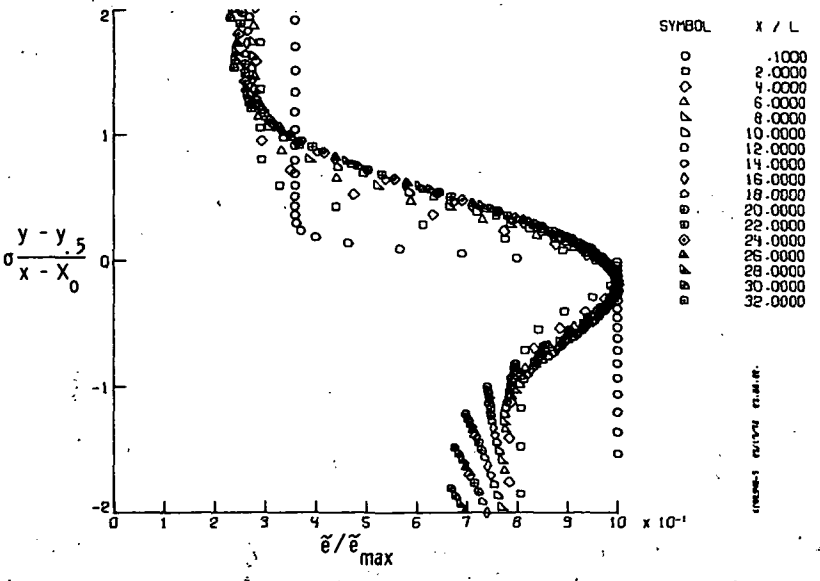

(j) Variation of $\tilde{e}/\tilde{e}_{max}$ with $\sigma(y - y_{.5})/(x - X_0)$. $X_0/L = -25.8005$; $\sigma = 19.7200$.

Figure 5.- Continued.

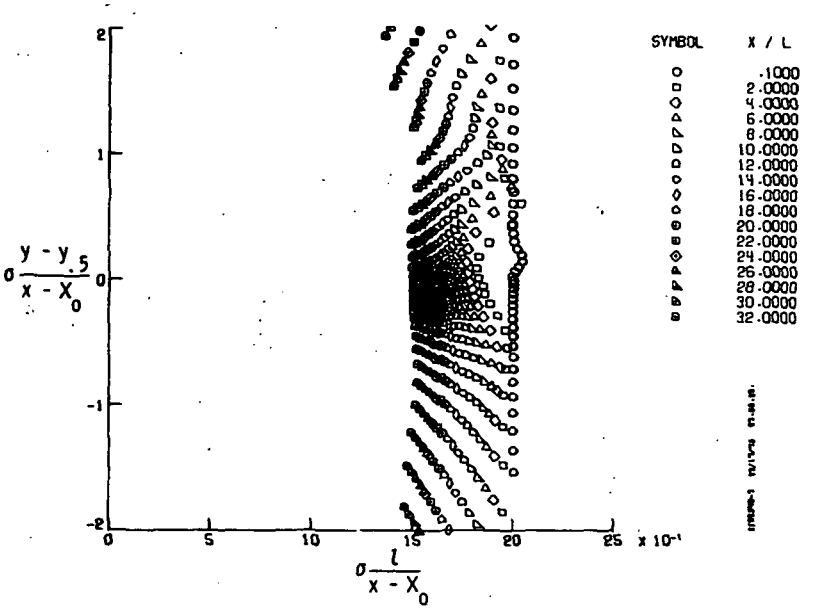

(k) Variation of $\sigma l/(x - X_0)$ with $\sigma(y - y_{.5})/(x - X_0)$. $X_0/L = -25.8005$; $\sigma = 19.7200$.

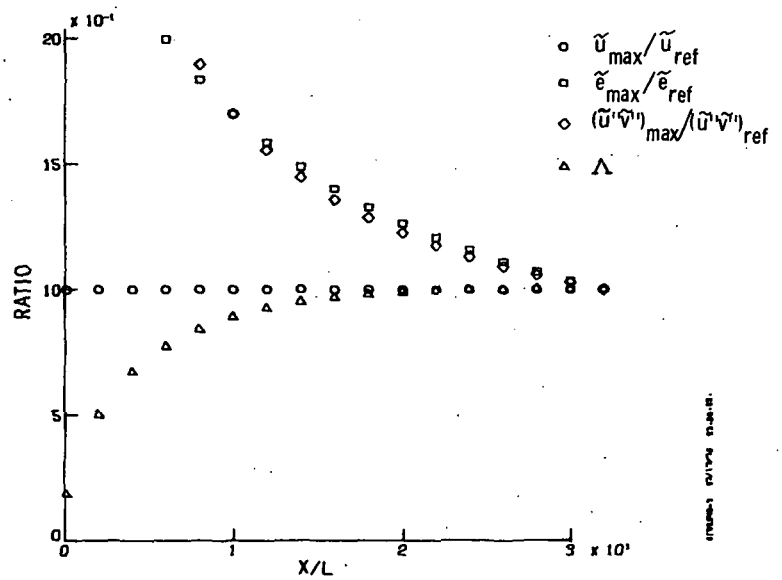

(l) Variation of $\tilde{u}_{max}/\tilde{u}_{ref}$, $\tilde{e}_{max}/\tilde{e}_{ref}$, $(\tilde{u}''\tilde{v}'')_{max}/(\tilde{u}''\tilde{v}'')_{ref}$, and Λ with x/L. $\sqrt{\tilde{e}_{ref}}/(\tilde{u}_1 - \tilde{u}_2) = \sqrt{0.0872}$; $(\tilde{u}''\tilde{v}'')_{ref}/(\tilde{u}_1 - \tilde{u}_2)^2 = 0.0242$; $L = \frac{10}{3}\delta_0$; $X_0/L = -25.8005$; $\sigma = 19.7200$.

Figure 5.- Continued.

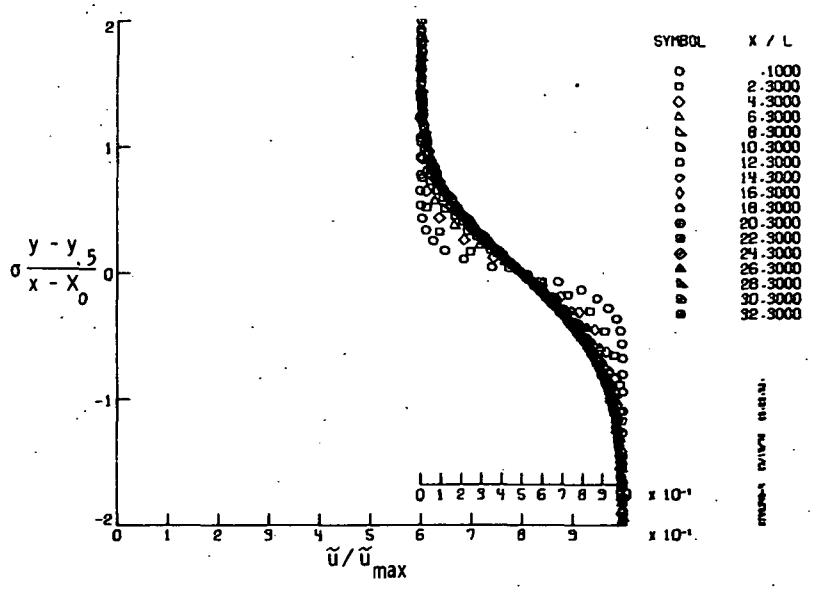

(m) Variation of $\tilde{u}/\tilde{u}_{max}$ with $\sigma(y - y_{.5})/(x - X_0)$ for $\tilde{u}_2/\tilde{u}_1 = 0.6$ with turbulence boundary conditions at $x = 0$; $\sqrt{\tilde{e}_\infty}/\tilde{u}_\infty = 0.02$; $l_\infty/\lambda = 10$; $L = \frac{10}{3}\delta_0$; $X_0/L = -16.6895$; $\sigma = 22.7909$.

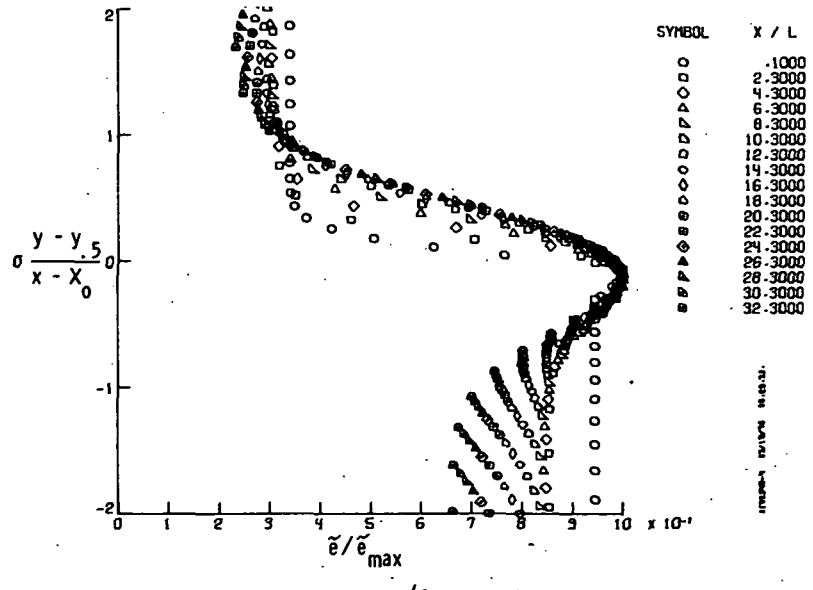

(n) Variation of $\tilde{e}/\tilde{e}_{max}$ with $\sigma(y - y_{.5})/(x - X_0)$. $X_0/L = -16.6895$; $\sigma = 22.7909$.

Figure 5.- Continued.

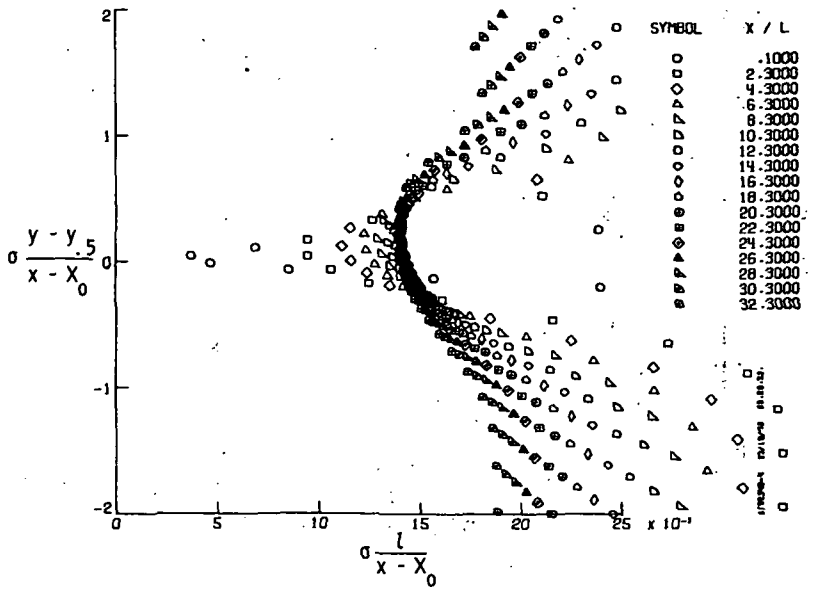

(o) Variation of $\sigma l/(x - X_o)$ with $\sigma(y - y_{.5})/(x - X_o)$. $X_o/L = -16.6895$; $\sigma = 22.7909$.

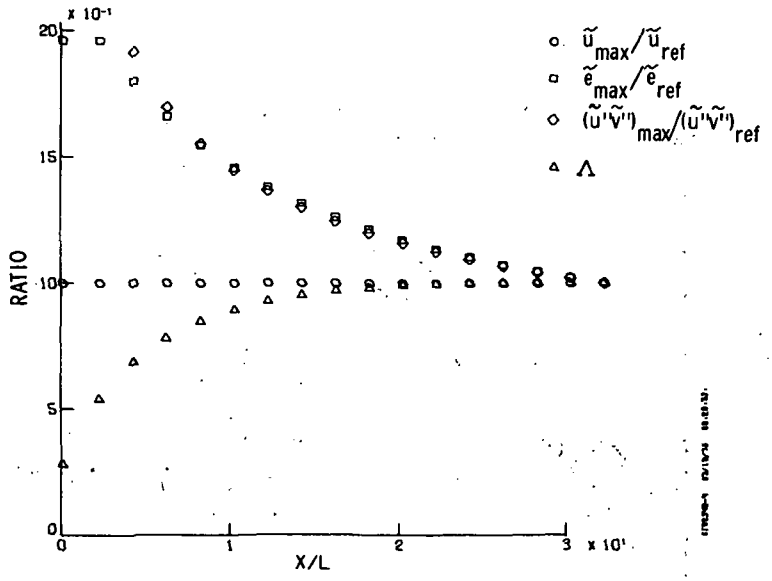

(p) Variation of $\tilde{u}_{max}/\tilde{u}_{ref}$, $\tilde{e}_{max}/\tilde{e}_{ref}$, $(\tilde{u}''\tilde{v}'')_{max}/(\tilde{u}''\tilde{v}'')_{ref}$, and Λ with x/L. $\sqrt{\tilde{e}_{ref}}/(\tilde{u}_1 - \tilde{u}_2) = \sqrt{0.0671}$; $(\tilde{u}''\tilde{v}'')_{ref}/(\tilde{u}_1 - \tilde{u}_2)^2 = 0.0213$; $L = \frac{10}{3}\delta_o$; $X_o/L = -16.6895$; $\sigma = 22.7909$.

Figure 5.- Concluded.

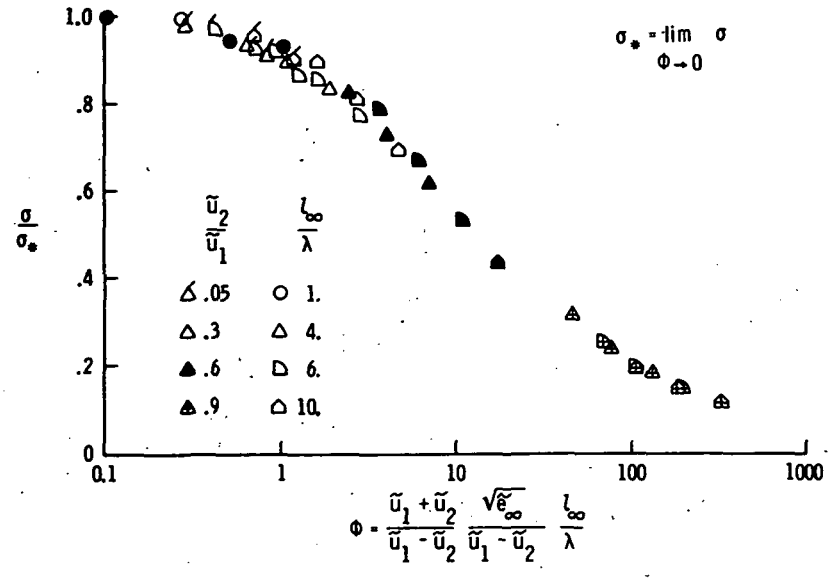

Figure 6.- Parametric correlation of predicted effect of wide-band free-stream disturbances (only one side) on turbulent free mixing (low speed). σ is based on width for 10 percent and 90 percent momentum.

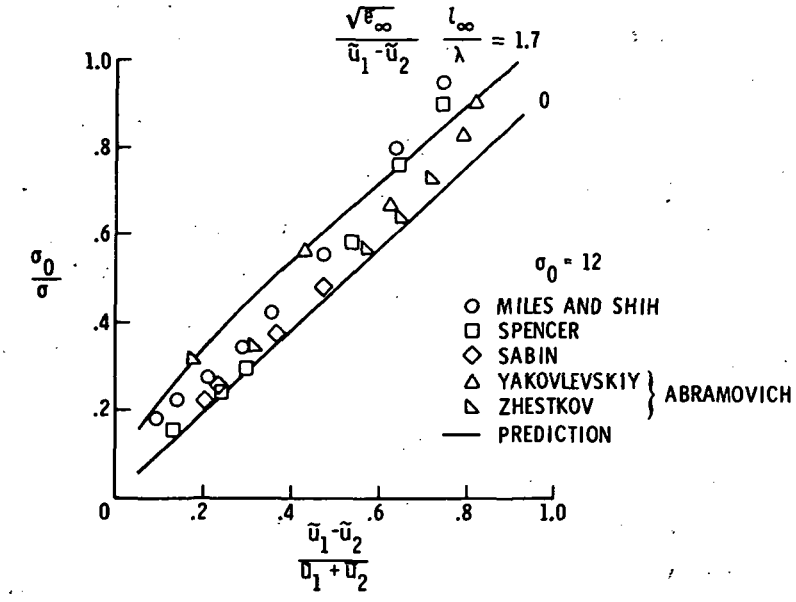

Figure 7.- Effect of wide-band free-stream disturbances. Variation of σ with $(\tilde{u}_1 - \tilde{u}_2)/(\tilde{u}_1 + \tilde{u}_2)$.

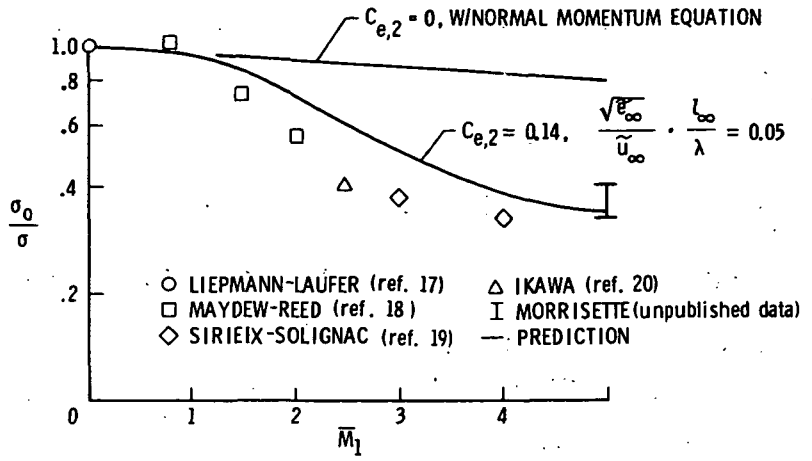

Figure 8.- Effect of Mach number on spreading rate prediction for clean flow.

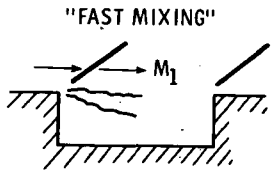

(a) Cavity Flows (refs. 22 and 23).

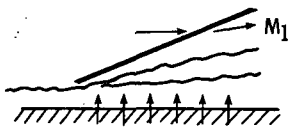

(b) Massive wall injection (ref. 24).

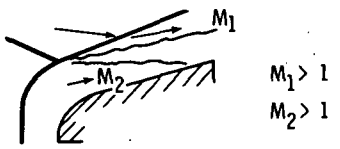

(c) Triple shock intersection (ref. 5).

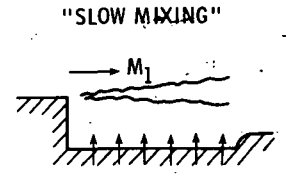

(d) Backward facing step with matched pressure (ref. 20).

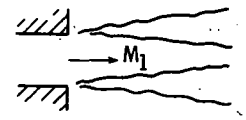

(e) Near field of isolated jets (ref. 21).

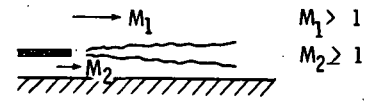

(f) Sonic slot injection into supersonic hypersonic flow (refs. 26 and 27) co-axial jet (ref. 28).

Figure 9.- Experimental configurations used for supersonic shear layer experiment.